

VSC-MMC STATION MODELS

MODULAR MULTILEVEL CONVERTER

in EMTP-RV

January 20, 2014

Prepared by:

Hani Saad and Jean Mahseredjian

École Polytechnique de Montréal, Canada

Sébastien Dennetière

Réseau de transport d'électricité, France

Table of Contents

1	ACKNOWLEDGEMENT	3
2	OBJECTIVE	3
3	INTRODUCTION.....	3
4	MMC STATION MODEL	6
4.1	OVERALL MODEL DESCRIPTION	6
4.2	STEP-UP TRANSFORMER.....	7
4.3	MAIN AC BREAKER.....	8
4.4	AC CONVERTER BREAKER	8
4.5	START POINT REACTOR	8
4.6	MODULAR MULTILEVEL CONVERT (MMC)	8
4.6.1	<i>Model 1 – Full Detailed.....</i>	<i>9</i>
4.6.2	<i>Model 2 - Detailed equivalent.....</i>	<i>10</i>
4.6.3	<i>Model 3 - Switching function of Arm</i>	<i>13</i>
4.6.4	<i>Model 4 - AVM based on power frequency.....</i>	<i>15</i>
4.7	CONTROL SYSTEM	16
4.7.1	<i>Principle of operation.....</i>	<i>16</i>
4.7.2	<i>Upper Level Control and Protection system.....</i>	<i>17</i>
4.7.3	<i>Upper Level Control.....</i>	<i>17</i>
4.7.4	<i>Lower Level Control.....</i>	<i>25</i>
4.8	PROTECTION SYSTEM	27
4.9	START-UP SEQUENCE.....	28
4.10	INITIAL CONDITIONS AND LOAD-FLOW SOLUTION	28
5	SIMULATION RESULTS	29
5.1	STEP CHANGE ON ACTIVE POWER REFERENCE	29
5.2	THREE-PHASE AC FAULT	30
5.3	POLE-TO-POLE DC FAULT.....	31
5.4	START-UP SEQUENCE.....	32
6	REFERENCES	35

1 Acknowledgement

The development of the models presented in this document was funded by RTE-France (Réseau de transport d'électricité).

2 Objective

The objective of this document is to present the Modular Multilevel Converter (MMC) Station model in EMTP-RV. The document describes the main components and control blocks of MMC station models. A comparison between different MMC modeling is also included for validation purposes.

3 Introduction

The development of controllable semiconductor switches and Voltage Source Converter (VSC) technologies is rapidly expanding the fields of applications of HVDC and FACTS in power systems. VSC-based HVDC systems present several advantages in comparison with traditional line-commutated converter (LCC) based HVDC transmission [1]. VSC-HVDC technology combines IGBT-based VSC with dc transmission lines to transfer power up to 1,000 MW [2]. The potential applications of VSC-HVDC systems include interconnections of asynchronous systems, grid integration of off-shore wind farms, electrification of remote islands, oil and gas stations, and multi-terminal dc grids [11]-[3]. VSC-HVDC systems can independently control both active and reactive powers by maintaining stable voltage and frequency [4] which enables the supply of very weak grids and even passive networks [5]. Various VSC topologies, including the conventional two-level, multi-level diode-clamped and floating capacitor multi-level converters, have been proposed and reported in [6]. However, due to the complexity of controls and practical limitations, the VSC-HVDC system installations have been limited to the two-level and three-level diode-clamped converters. Recently, the development of the Modular Multilevel Converter (MMC) technology with series-connected half-bridge modules, has overcome the limitations of other multilevel converter topologies for HVDC applications [7]. MMC topologies allow using a lower switching frequency for reducing converter losses. In addition, filter requirements are eliminated by using a significant number of levels per phase. Scalability to higher voltages is easily achieved and reliability is improved by increasing the number of sub-modules (SMs) per arm [8].

In the EMTP-RV model, two types of MMC station configurations are available: Monopole configuration (Figure 1) and Bipole with earth grounding return (Figure 2). The Bipole configuration is composed from two identical Monopole configurations connected at ac and dc sides (see Figure 2).

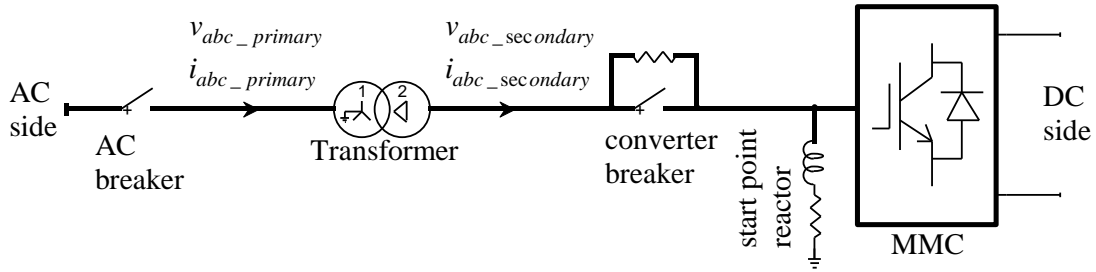


Figure 1: Typical Monopole Configuration of a MMC station

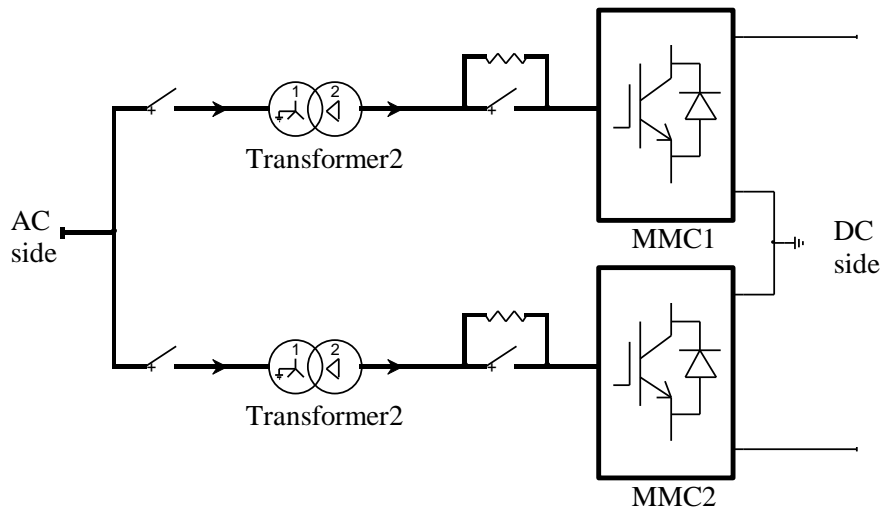


Figure 2: Bipole with earth grounding return Configuration of a MMC station

Figure 3.a shows the three-phase configuration of the MMC topology. This MMC model is based on the preliminary MMC-HVDC system design for the planned interconnection between France and Spain 400 kV networks in 2013 [9][10]. The MMC is comprised of N SMs per arm which results into a line-to-neutral voltage waveform of $(N+1)$ levels [10]. The inductor L_{arm} is added on each arm to limit arm-current harmonics and fault currents. Each SM is a half-bridge converter as depicted in Figure 3.b and includes mainly a capacitor C and two IGBTs with antiparallel diodes (S1 and S2).

Since the IGBT device is controllable, through gate signals g_{1_i} and g_{2_i} , the SM can have three different states. In the ON state: g_{1_i} is on, g_{2_i} is off and the SM voltage v_{SM_i} is equal to the capacitor voltage v_{C_i} . In the OFF state: g_{1_i} is off, g_{2_i} is on and $v_{SM_i} = 0$. In the Blocked state: g_{1_i} is off, g_{2_i} is off and v_{SM_i} depends on the arm current (i_{arm}) direction. The capacitor may charge through S1 and cannot discharge.

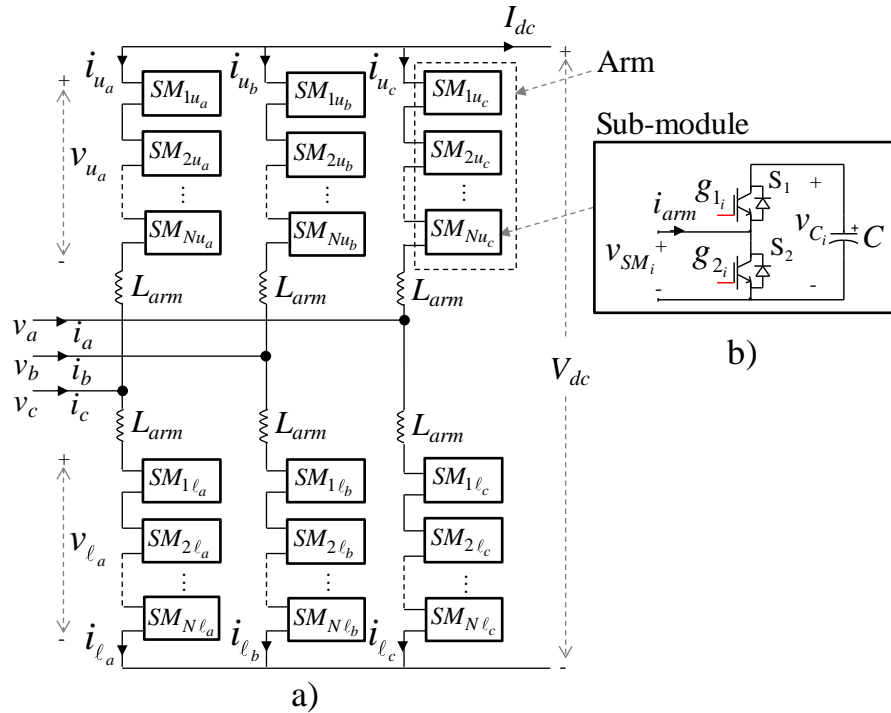


Figure 3: a) MMC topology b) Half-bridge converter for the \$i\$th SM

Since the MMC topology is of VSC type [13], it uses an upper level control similar to the previous VSC technology. However, the MMC topology requires additional controllers in order to stabilize internal variables (Lower Level Control): SM capacitor voltages, second harmonic circulating currents of each phase and modulation technique [18][14]. A top level view of the control structure is presented in Figure 4.

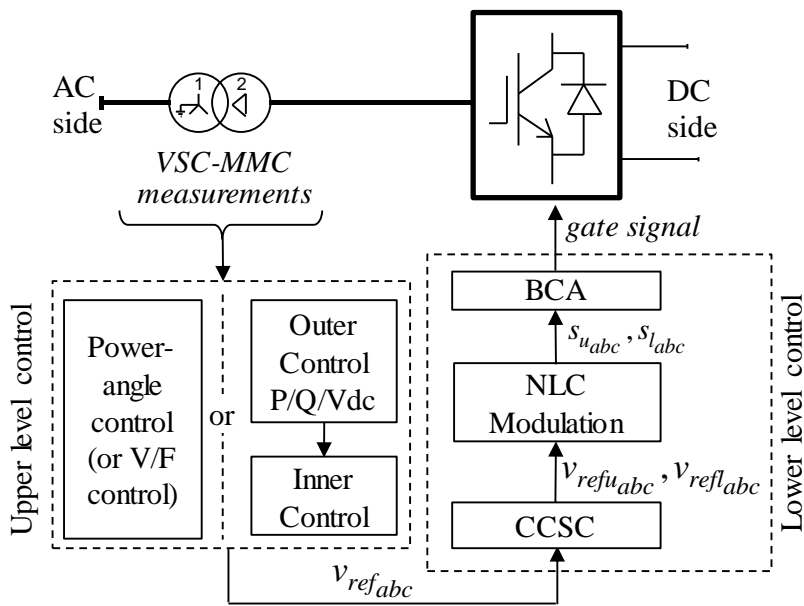


Figure 4: Control hierarchy for the MMC station

Several control methods are available for Upper Level Control. Among them the power-angle and vector-current controls are the mostly widely used. The principle of power-angle control is simple. The active power is controlled by the phase-angle shift between the VSC and the ac system, while the reactive power is controlled by varying the VSC voltage magnitude [15]. Power-angle control (or V/F control) is used when the VSC converter is connected to an ac system with passive load or for wind-turbine applications [11]. Vector-current control [4] is a current-control-based technology. Thus, it can naturally limit the current flowing into the converter during disturbances. The basic principle of vector-current control is to regulate the instantaneous active and reactive powers independently through a fast inner current control loop. By using a dq decomposition technique with the grid voltage as phase reference, the inner current control loop decouples the current into d and q components, where outer loops can use the d component to control active power or dc voltage, and the q component to control reactive power or ac voltage. Due to its successful application in HVDC transmission system, vector-current control has become the dominant control method for grid-connected VSCs in almost all applications today [17].

4 MMC station model

This section describes the main components and control system of the MMC station model available in EMTP-RV.

4.1 Overall Model Description

The model is a 1,060 MVA MMC station connected to a 400 kV ac system at the Point of Common Coupling (PCC) through a 400/320 kV step-up transformer and 640 kV pole-to-pole dc voltage, as shown in Figure 5. It should be noted that these parameters can be modified in the main mask.

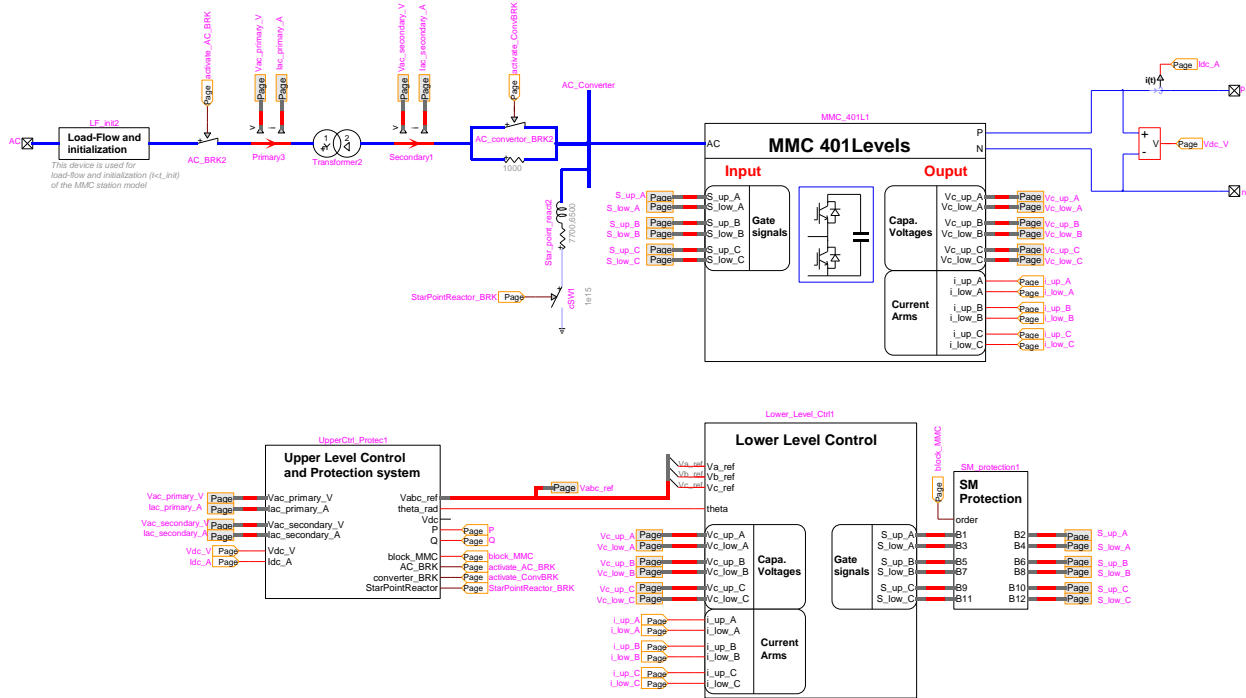


Figure 5: MMC station – EMTF-RV

The main components of the MMC station include:

- Initialization and load-flow system to represent the MMC station for load-flow solution.
- Step-up transformer
- The main ac breaker
- Star point reactor
- AC converter breaker and the insertion resistance for start-up procedure
- The ac/dc converter based on Modular Multilevel Converter (MMC) technology
- Control and protection system composed from the Upper and Lower Level control.

A detailed description of each component is presented in the following sections.

4.2 Step-up transformer

The MMC is connected to the ac grid through a step-up transformer. The transformer connection is wye-grounded on the primary side (ac grid) and Delta on the secondary side (converter side). The transformer impedance has a value of 18% and can be configured from the main mask. In this version the remaining parameters can be configured from the MMC_m.dwj file found in the Toolboxes\MMC folder.

4.3 Main ac breaker

The main ac breaker is used to connect the MMC station to the ac grid. During normal operation, the ac breaker is closed. The breaker is controlled from the protection system. If the protection system is active and a dc overcurrent is detected, the MMC station is tripped (by opening the ac breaker) and the MMC is blocked.

4.4 AC converter breaker

The ac converter breaker is used for the start-up sequence. When it is open, the insertion resistance (connected in parallel) will limit the current flowing into the MMC. If the start-up sequence is unchecked, the ac converter breaker is always closed.

4.5 Start point reactor

Since the secondary winding of the transformer has a Delta connection, the start point reactor is used to give to the MMC a reference to ground.

4.6 Modular Multilevel Convert (MMC)

The large number of IGBTs in MMCs complicates the simulations in electromagnetic transient type (EMT-type) simulation tools. Detailed MMC models must include the representation of thousands of IGBTs and small numerical integration time steps are required to accurately represent fast and multiple simultaneous switching events. The excessive computational burden introduced by such models highlights the need to develop more efficient models. A current trend is based on simplified and averaged value models capable of delivering sufficient accuracy [19] in dynamic simulations.

Average Value Models (AVMs) approximate system dynamics by neglecting switching details [20]. They require significantly less computational resources and can use larger integration time steps leading to much faster computations.

Circuit reduction is achieved by the replacement of IGBTs by on/off resistors in the SMs. The equivalent circuit usage allows reducing the number of operations and improving computational performance.

Four types of MMC models are available in EMTP-RV. These models can be used according to the type of study and required accuracy. MMC model evolution in decreasing complexity is depicted in Figure 6. Black boxes represent simplifications of each model. It is expected, that by decreasing model complexity, computational performance can be increased.

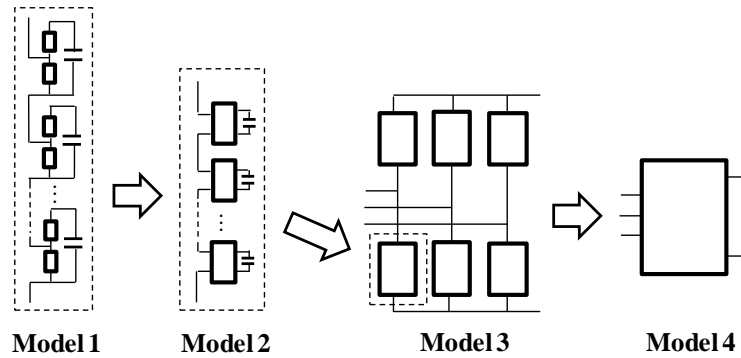


Figure 6: MMC model evolution in decreasing complexity

The model details are presented in the next sections.

4.6.1 Model 1 – Full Detailed

This model is based on nonlinear IGBT representation. It is the most accurate model and can account for every conduction mode of the MMC. This model requires the highest computational time. It can be used for advanced studies, prototyping different SM circuit topologies and to validate results obtained with simplified models listed below [18]. It can be also used to calibrate parameters in simplified models. Figure 7 shows the subcircuit hierarchy of a full detailed model of MMC-401L (i.e. 400SM/arm).

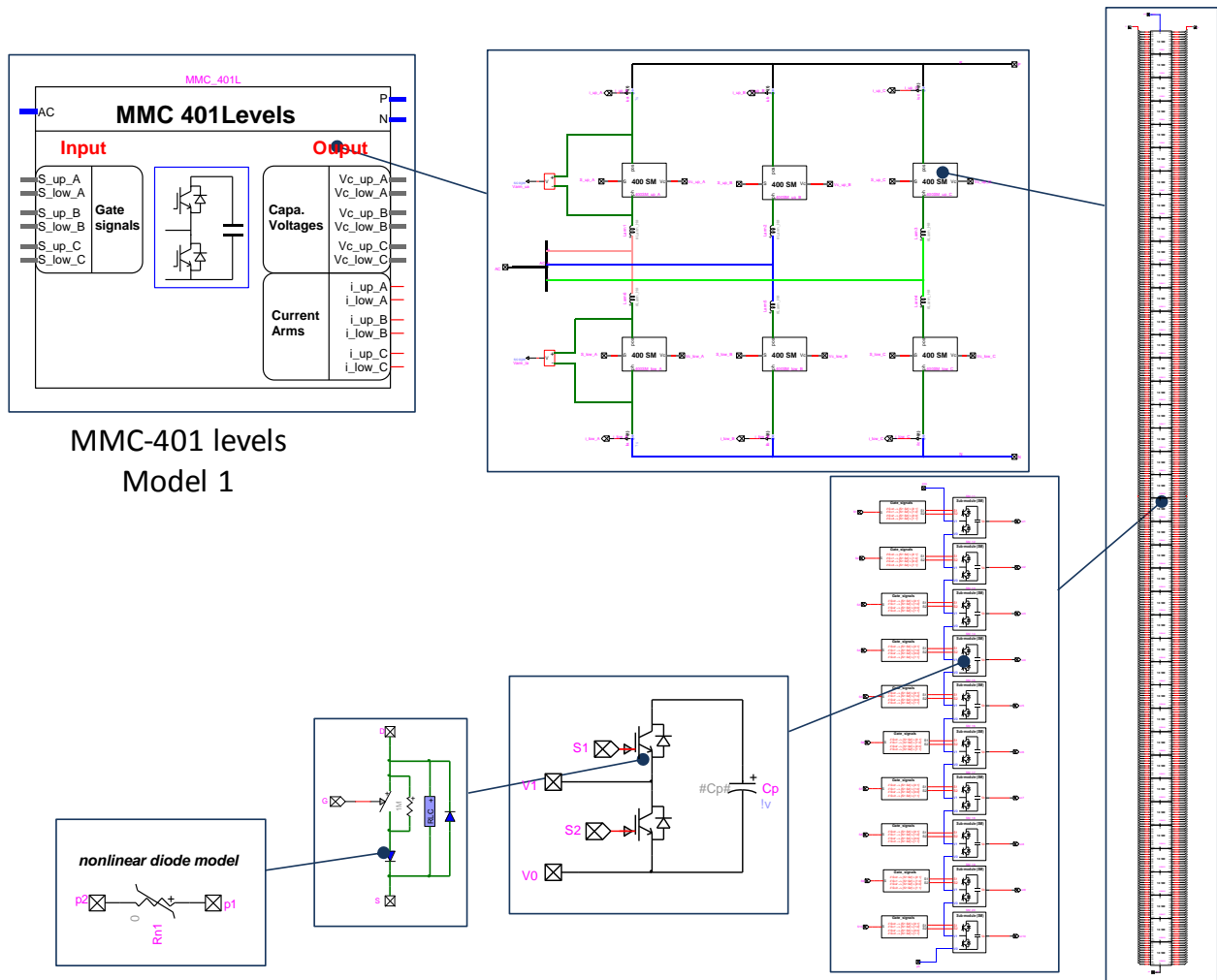


Figure 7: Subcircuit hierarchy of Model 1-Full Detailed for a MMC-401L

For this type of model, three MMC levels are available in EMTP-RV and can be set from the main mask: MMC-401L (400SM/arm), MMC-101L (100SM/arm) and MMC-21L (20SM/arm).

4.6.2 Model 2 - Detailed equivalent

In this model the SM power switches are replaced by ON/OFF resistors: R_{ON} (small value in m Ω) and R_{OFF} (large value in M Ω). This approach allows performing an arm circuit reduction for eliminating internal electrical nodes and allowing the creation of a Norton equivalent for each MMC arm. R_1 and R_2 are controlled and used for replacing the two IGBT/diode combinations. With the trapezoidal integration rule, each SM capacitor is replaced by an equivalent current history source $i_{C_i}^h(t - \Delta t)$ in parallel with a resistance $R_C = \Delta t / (2C)$ (Figure 8), where Δt is the numerical integration time-step. The derivation of these equations and the block station conditions can be found in [21].

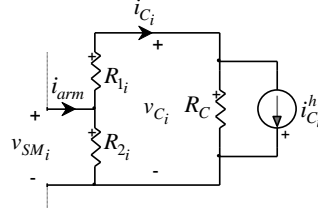


Figure 8: Discretized SM with simplified IGBT/diode models

Table 1 shows the algorithm used for Model 2. In point 2 of Table 1, it can be seen that the computation of ON/OFF states is straight forward since only gate signal values are required. When the Blocked state is set, only the freewheeling diodes can conduct. The diode conduction states depend on voltage and current variables (Table 1 point 2) that are known only from the previous iteration ($v_{SM_i}(t_{-1})$ and $v_{C_i}(t_{-1})$).

Table 1: MMC arm algorithm of Model 2

1. Retrieve $v_{arm}(t)$ from network solution and compute $i_{arm}(t)$
2. For $i = 1, 2, \dots, N$ Set R_{1_i} and R_{2_i} values: if (SM_i is ON) $\{R_{1_i} = R_{ON}; R_{2_i} = R_{OFF}\}$ elseif (SM_i is OFF) $\{R_{1_i} = R_{OFF}; R_{2_i} = R_{ON}\}$ elseif (SM_i is Blocked) { if ($(i_{arm}(t) > 0)$ and ($v_{SM_i}(t_{-1}) > v_{C_i}(t_{-1})$)) $\{R_{1_i} = R_{ON}; R_{2_i} = R_{OFF}\}$ if ($(i_{arm}(t) < 0)$ and ($v_{SM_i}(t_{-1}) < 0$)) $\{R_{1_i} = R_{OFF}; R_{2_i} = R_{ON}\}$ else $\{R_{1_i} = R_{OFF}; R_{2_i} = R_{OFF}\}$ } Compute $v_{C_i}(t)$ and $i_{C_i}(t)$ Compute Thevenin equivalent of each SM Compute SM voltages for next iteration: $v_{SM_i}(t)$
3. Compute and send Norton equivalent of the arm

When the Blocked state is set for one of the SMs and a change in conduction state of one of the diodes is detected, the EMTP-RV iterative process is activated in the current time-step in order to find the correct conduction states and the trapezoidal integration rule is switched to the Backward Euler method for the next time-step (see Figure 9).

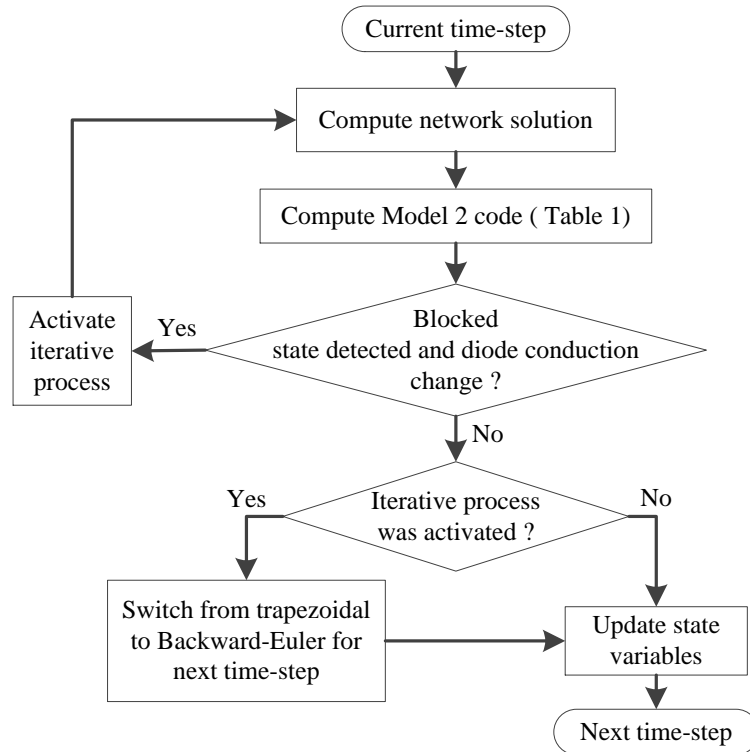


Figure 9: Bloc diagram, iterative process used for Model 2

The main advantage of Model 2 is the significant reduction in the number of electrical nodes in the main system of network equations. The algorithm still considers each SM separately and maintains a record for individual capacitor voltages. Figure 10 presents the subcircuit hierarchy of model 2.

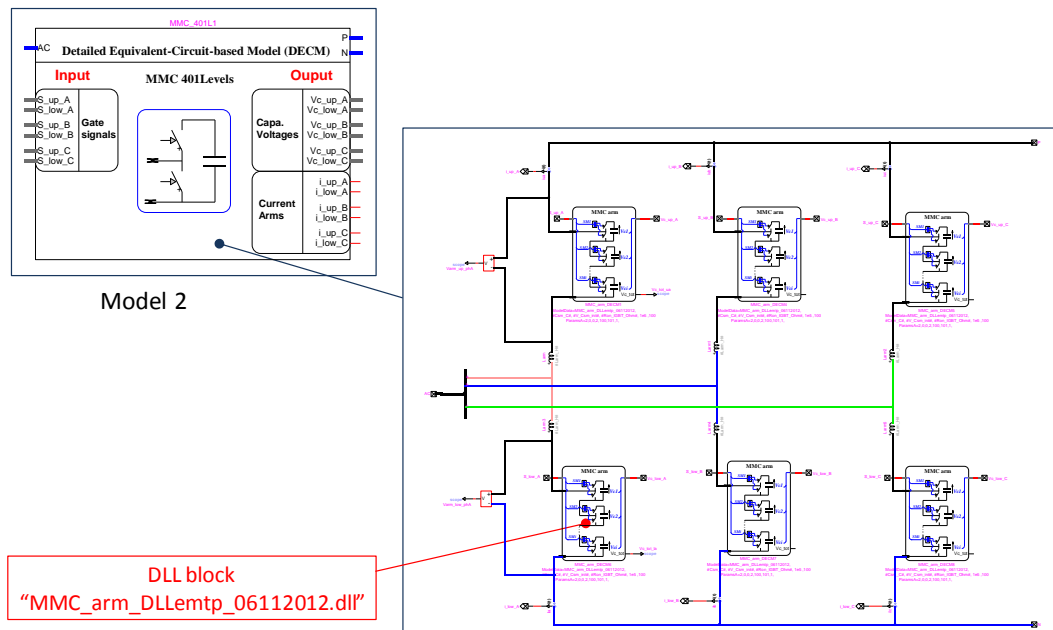


Figure 10: Subcircuit hierarchy of Model 2-Detailed Equivalent for a MMC-401L

For this type of model, three MMC levels are available in EMTP-RV and can be set from the main mask: MMC-401L (400SM/arm), MMC-101L (100SM/arm) and MMC-21L (20SM/arm).

4.6.3 Model 3 - Switching function of Arm

In this model each MMC arm is averaged using the switching function concept of a half-bridge converter. Let S_i be the switching function which takes the value 0 when the state of SM is OFF and 1 when it is ON. For each SM

$$\begin{aligned} v_{SM_i} &= S_i v_{C_i} \\ i_{C_i} &= S_i i_{arm} \end{aligned} \quad (1)$$

Assuming that capacitor voltages of each arm are balanced, the average values of capacitor voltages are equal. In addition, by neglecting the voltage differences between capacitors, the following assumption can be made:

$$v_{C_1} = v_{C_2} = \dots = v_{C_i} = \frac{v_{C_{tot}}}{N} \quad (2)$$

where $v_{C_{tot}}$ represents the sum of all capacitor voltages of an arm. The accuracy of assumption (2) increases when the number of SMs per arm is increased and/or when the fluctuation amplitudes of capacitor voltages are decreased. This assumption allows deducing an equivalent capacitance $C_{arm} = C/N$ for each arm.

By defining the switching functions of an arm as follows:

$$\frac{1}{N} \sum_{i=1}^N S_i = s_n \quad (3)$$

and including the linear conductivity losses (R_{ON}) for each SM, the following switching functions can be derived for each arm when the SMs are in ON/OFF states:

$$\begin{aligned} v_{arm} &= s_n v_{C_{tot}} + (NR_{ON}) i_{arm} \\ i_{C_{tot}} &= s_n i_{arm} \end{aligned} \quad (4)$$

where v_{arm} is the arm voltage. Half-bridge converters are non-reversible in voltage. In order to avoid negative voltages, a diode D is added in parallel with the equivalent capacitor (Figure 11.a).

When all SMs are in the Blocked state, each MMC arm can be simply represented by an equivalent half-bridge diode connected to the equivalent capacitor (Figure 11.b).

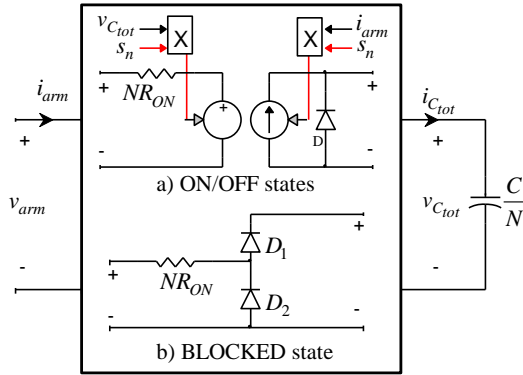


Figure 11: Switching function model of MMC arm: a) ON/OFF states model, b) Blocked state model

By reducing each arm to an equivalent switching function model, the SMs are no longer represented. This means that the balancing controls of capacitor voltages in each arm and redundant SM impacts cannot be studied using this approach. However, circulating currents and the linear conduction losses can be represented. Moreover, the energy transferred from ac and dc sides into each arm of the MMC is taken into account, which is useful for control system strategies based on internal MMC energy balance.

Since this model includes two circuit models (see Figure 11), its implementation in EMT-type programs is hard-coded, using a DLL block, to increase computational performance. Depending on the states of each arm, the adequate circuit is interfaced with the main network.

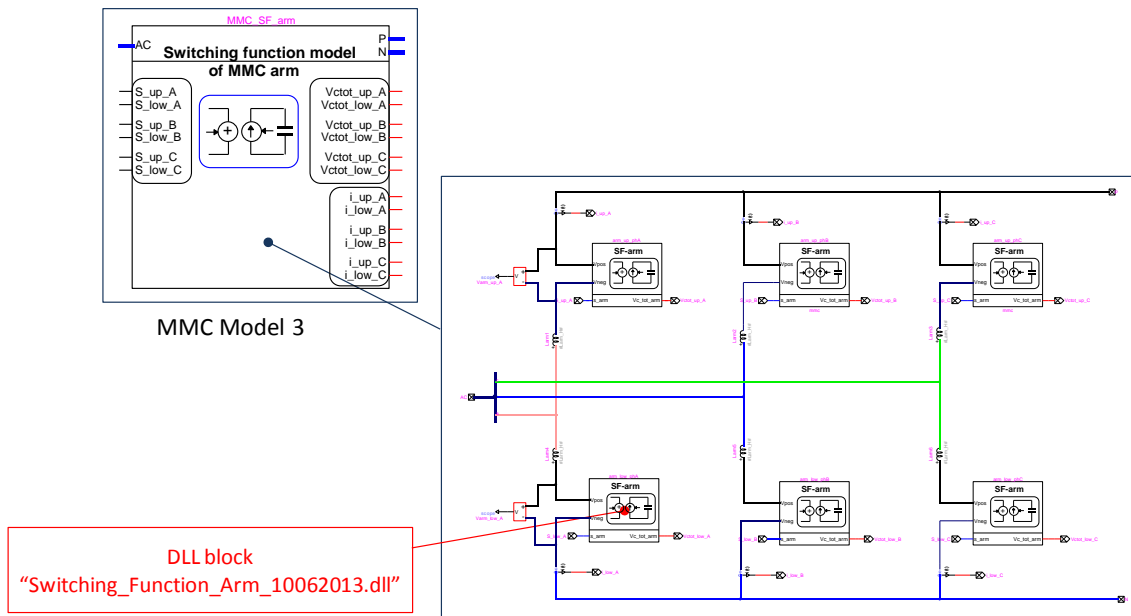


Figure 12: Subcircuit hierarchy of Model 3-Switching function, MMC arm

For this type of model, any number of MMC levels can be represented in EMT-PV and can be set from the main mask.

4.6.4 Model 4 - AVM based on power frequency

In the average value model (AVM), the IGBTs and their diodes are not explicitly represented and the MMC behavior is modeled using controlled voltage and current sources. The classical AVM approach developed for 2 and 3 level VSCs in [22] is extended to MMCs in [9]. It is used by assuming that the internal variables of the MMC are perfectly controlled, i.e. all SM capacitor voltages are perfectly balanced and second harmonic circulating currents in each phase are suppressed. Based on the approach presented in [9], the following equation can be derived from Figure 3 for each phase $j = a, b, c$

$$v_{convj} = \frac{L_{arm}}{2} \frac{di_j}{dt} - v_j \quad (5)$$

Assuming that the total number of inserted SMs in each phase is constant and since the circulating current is assumed to be zero,

$$v_{uj} + v_{lj} = V_{dc} \quad (6)$$

With the above equations (5) and (6), the MMC can be represented as a classical VSC (2 and 3 level topologies). Thus, using an approach similar to [22], the controlled voltage sources become:

$$v_{convj} = v_{refj} \frac{V_{dc}}{2} \quad (7)$$

where v_{refj} are the voltage references generated from the inner controller. The dc side model is derived using the principle of power balance, thus it assumes that no energy is stored inside the MMC converter:

$$V_{dc} I_{dc} = \sum_{j=a,b,c} v_{convj} i_j \quad (8)$$

The dc current function is derived from(7):

$$I_{dc} = \frac{1}{2} \sum_{j=a,b,c} v_{refj} i_j \quad (9)$$

The equivalent capacitor C_{dc} (shown in Figure 13) is derived using the energy conservation principle [9] and it is given by $C_{dc} = 6C/N$.

Unlike the classical VSC model, an inductance is included in each arm of the MMC, thus an equivalent inductance should be also added on the dc side. Since one third of the dc current flows in each arm and the same dc current flows in upper and lower arms of each phase, the equivalent inductance is given by $L_{arm_{dc}} = (2/3)L_{arm}$. The total conduction losses of the MMC can be found using $R_{loss} = (2/3)N R_{ON}$. The implementation of Model 4 in EMTP-RV is presented in Figure 13

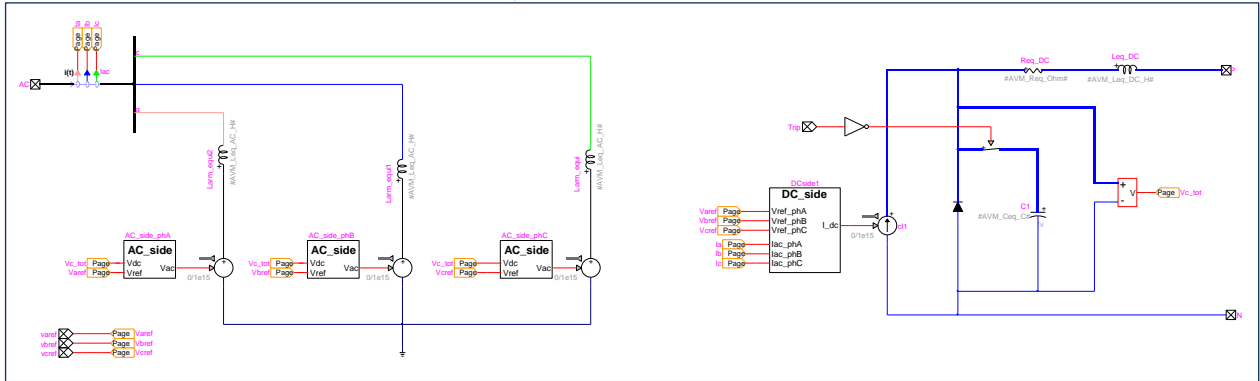
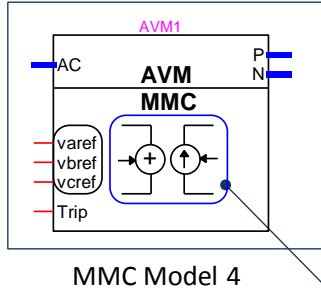


Figure 13: Subcircuit hierarchy of Model 4-AVM

4.7 Control System

Since the MMC topology is of VSC type [13], it uses an upper level control similar to the previous VSC technology.

4.7.1 Principle of operation

In order to understand the principle of the VSC-MMC control system, let us first consider the two bus system (Figure 14), where V_s is the ac voltage source, V_{conv} is the ac voltage of the converter and X is the equivalent inductance between the ac source and converter (i.e. transformer leakage inductance, equivalent arm inductance, etc.). The losses are neglected for simplification purposes. The transferred active and reactive powers from the source to the converter are given by the following relationships:

$$\begin{aligned}
 P_R &= \frac{V_S V_{conv}}{X} \sin(\delta) \\
 Q_R &= \frac{V_S V_{conv} \cos(\delta) - V_{conv}^2}{X}
 \end{aligned} \tag{10}$$

where δ is the angle between the two voltages.

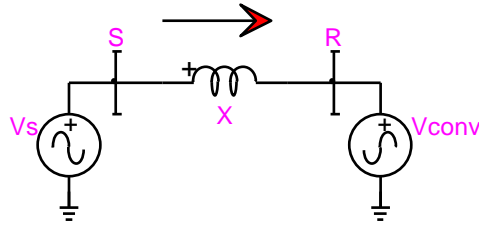


Figure 14: Two-bus system representing the functionality of the VSC-MMC control system

Assuming that the angle δ is small, the power equations (10) can be linearized as follow:

$$P_R \approx \frac{V_S V_{conv}}{X} \delta$$

$$Q_R \approx \frac{V_{conv} (V_S - V_{conv})}{X}$$
(11)

From (11), one can see that by controlling the voltage amplitude and phase angle of the converter, it is then possible to regulate the active and reactive powers at a desired set-point.

4.7.2 Upper Level Control and Protection system

The contents of the UpperCtrl_Protect block are presented in Figure 15. All measured signals entering the control system are, first, converted to pu (Convert_to_pu bloc) and then filtered by means of a Low-pass filter with a cut-off frequency equal to 2kHz (LP_filter bloc). The UpperCtrl block includes the Upper Level Control system that will be described in the next section. The Protect_StartUp block includes the dc overcurrent and Deep Voltage Sag detectors for protecting the converter and the start-up sequence devices.

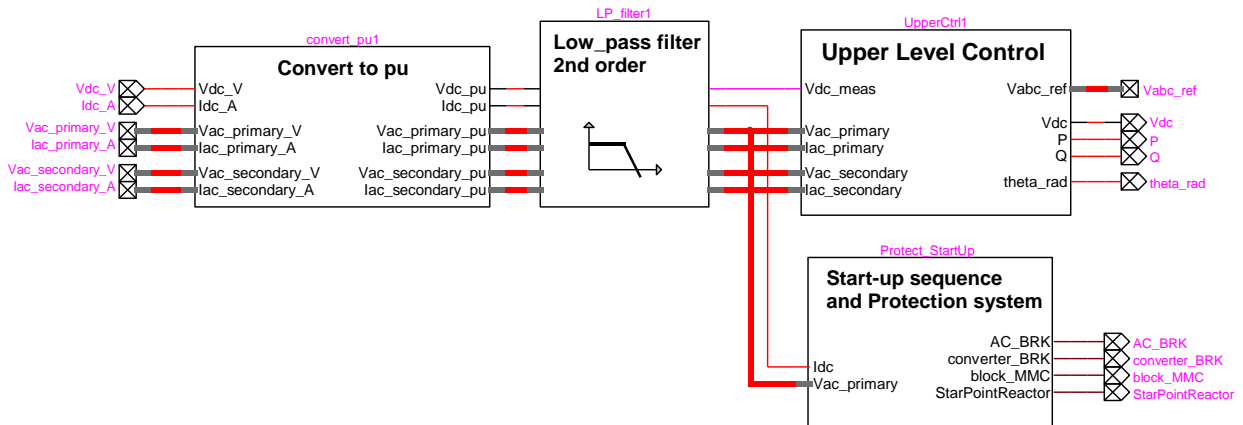


Figure 15: Upper Level Control and Protection System

4.7.3 Upper Level Control

The UpperCtrl block is presented in Figure 16. As previously mentioned, all variables are in pu except for the theta angle that is in radians.

The three following blocks: Clarke_transfo, signal_calculations and dq_transfo compute the required variables needed for the control system. Clarke transformation is implemented in the Clarke_transfo block. AC voltage, active and reactive powers are computed in the signal_calculations block. The dq_transfo block is used to extract the dq components from the three-phase ac voltages and currents.

The transformation matrix T in equation (12) transforms the three-phase variables (voltages and currents) to two quadrature axis (d and q reference frame) components rotating at synchronous speed $w = d\theta / dt$. The phase angle θ is derived, found by means of an internal oscillator (if V/F control is selected from the main mask) or found by the PLL allowing the synchronization of control parameters with the system voltage. In the matrix T , the direct axis d is aligned with the grid voltage.

$$T = \frac{2}{3} \begin{bmatrix} \cos(\omega t) & \cos(\omega t - 2\pi/3) & \cos(\omega t + 2\pi/3) \\ -\sin(\omega t) & -\sin(\omega t - 2\pi/3) & -\sin(\omega t + 2\pi/3) \\ 1/2 & 1/2 & 1/2 \end{bmatrix} \quad (12)$$

Using the transformation matrix T , the dq voltage and current variables can be deduced:

$$i_{dq} = T i_{abc} \quad (13)$$

$$v_{dq} = T v_{abc_grid} \quad (14)$$

The active and reactive powers and the ac grid voltage (in pu) are calculated from the dq reference as follows:

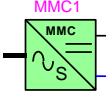
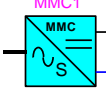
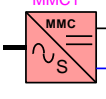
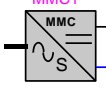
$$P = v_d i_d + v_q i_q \quad (15)$$

$$Q = -v_d i_q + v_q i_d \quad (16)$$

$$v_{grid} = \sqrt{v_d^2 + v_q^2} \quad (17)$$

Two main structures of upper level controls exist (see Figure 4): V/F control (or power-angle control) represented by the VFcontrol block and vector-current control represented by the Outer_control and Inner_control (Figure 16). The regulations of variables are performed through a PI control loop. All PI controllers are equipped with anti-windup function. This later will prevent the integral part from the accumulation of errors when the output value reaches the limit set by the user and enhances control performances [23]. The integral and proportional gains of each PI controller are automatically calculated based on the settling time (within 5% of error) chosen by the user. These settling times (or constant times) can be modified in the main mask. The background color of the MMC station block changes automatically depending on the selected type (see Table 2).

Table 2 Assigned background colors for each Outer control type

Outer Controller Type	Assigned Color for MMC model
Active Power Control (Green color)	
DC voltage Control (Cyan color)	
P/Vdc Droop Control (Pink color)	
V/F control (Gray color)	

A detailed description of each control block is provided in the following sections.

The selector block is used to switch automatically between vector-current control and V/F control depending on the outer control type chosen by the user from the main mask.

The Synchronization block is required for synchronization with the ac grid. It includes PLL and the internal oscillator. The Linearization_dq2abc block is for linearization and converts from dq to abc reference.

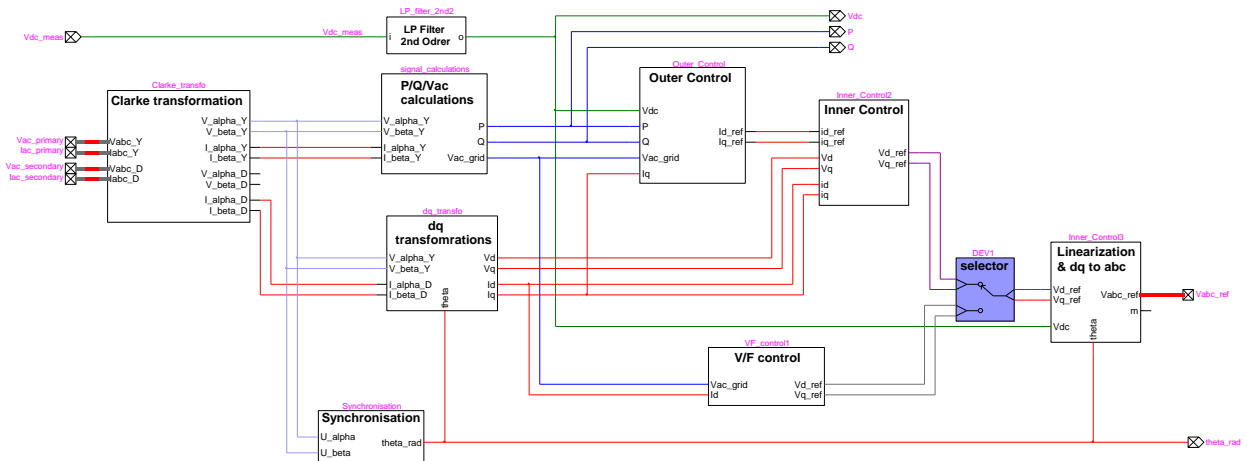


Figure 16: Upper Level Control block

4.7.3.1 V/F control (Vac/f control)

To produce three-phase ac voltages, the converter needs three variables: magnitude, phase angle and frequency. In the V/F control, the phase angle and frequency are generated from the internal oscillator (see Synchronisation/oscillator bloc). However the ac voltage magnitude is controlled by means of a PI control. The control law is

$$\Delta v_{grid} = \left(k_p + \frac{k_i}{s} \right) (v_{ref} - v_{grid}) \quad (18)$$

Only the integer part is used in the presented EMTP-RV model; however user can use also a PI control. The tuning of the integral gain (VFctrl_ki) is dependent from the ac grid impedance at PCC.

As grid voltage vector is aligned with the d axis and based on [24], the following equation can be driven:

$$v_{d_ref} = (V_0 + \Delta v_{grid}) + H_{HP}(s) i_d \quad (19)$$

$$v_{q_ref} = 0 \quad (20)$$

where V_0 is the nominal voltage (equal to v_{ref}), $H_{HP}(s)$ is a high-pass filter and the term $H_{HP}(s) i_d$ is used for damping (further information can be found in [24]). The VF_control block is shown in Figure 17.

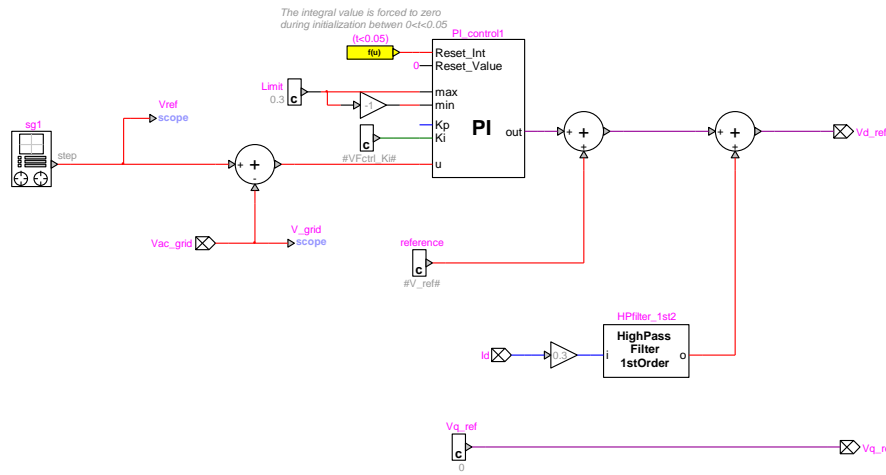


Figure 17: V/F control (Vac/f control)

V/F control is usually used when the VSC converter is connected to an ac system with passive load or for wind-turbine applications.

4.7.3.2 Vector-current control (Outer/Inner control)

Outer_control and Inner_control blocks represent the vector-current control. The basic principle of vector-current control is to regulate the instantaneous active and reactive powers independently through a fast inner current control loop. By using a dq decomposition technique with the grid voltage as phase reference, the inner current control loop decouples the current into d and q components, where outer loops can use the d component to control active power (P control) or dc voltage (Vdc control), and the q component to control reactive power (Q control) or ac voltage (Vac control). One of the main advantages of this control system is his ability to limit the current flowing into the converter during disturbances. Due to its successful application in HVDC transmission system, vector-current control has become the dominant control method for grid-connected VSCs in almost all applications today [17].

Using the current sign convention from Figure 1 and Figure 3 (current entering into the MMC) and neglecting the start point reactor, the following equations can be written for each phase $j = a, b, c$

$$\frac{V_{dc}}{2} = v_{u_j} + L_{arm} \frac{di_{u_j}}{dt} + R_{arm} i_{u_j} - L_{transfo} \frac{di_j}{dt} - R_{transfo} i_j + v_{grid_j} \quad (21)$$

$$\frac{V_{dc}}{2} = v_{\ell_j} + L_{arm} \frac{di_{\ell_j}}{dt} + R_{arm} i_{\ell_j} + L_{transfo} \frac{di_j}{dt} + R_{transfo} i_j - v_{grid_j} \quad (22)$$

The following variable is defined

$$v_{conv_j} = \frac{v_{\ell_j} - v_{u_j}}{2} \quad (23)$$

Using (23) and subtracting (21) and (22):

$$v_{grid_j} - v_{conv_j} = \left(\frac{L_{arm}}{2} + L_{transfo} \right) \frac{di_j}{dt} + \left(\frac{R_{arm}}{2} + R_{transfo} \right) i_j \quad (24)$$

By applying Park transformation, (24) becomes:

$$v_{conv_d} = -\left(i_{ref_d} - i_d \right) \left(k_p + \frac{k_i}{s} \right) + v_d + \left(\frac{L_{arm}}{2} + L_{transfo} \right) \omega i_q \quad (25)$$

$$v_{conv_q} = -\left(i_{ref_q} - i_q \right) \left(k_p + \frac{k_i}{s} \right) + v_q - \left(\frac{L_{arm}}{2} + L_{transfo} \right) \omega i_d$$

The inner controller is presented in Figure 18 and permits controlling the reference voltages (V_d_ref and V_q_ref) that will be used for the Lower Level Control. In order to decouple the d- and q-axis, a feed-forward technique is used to compensate cross-coupling terms.

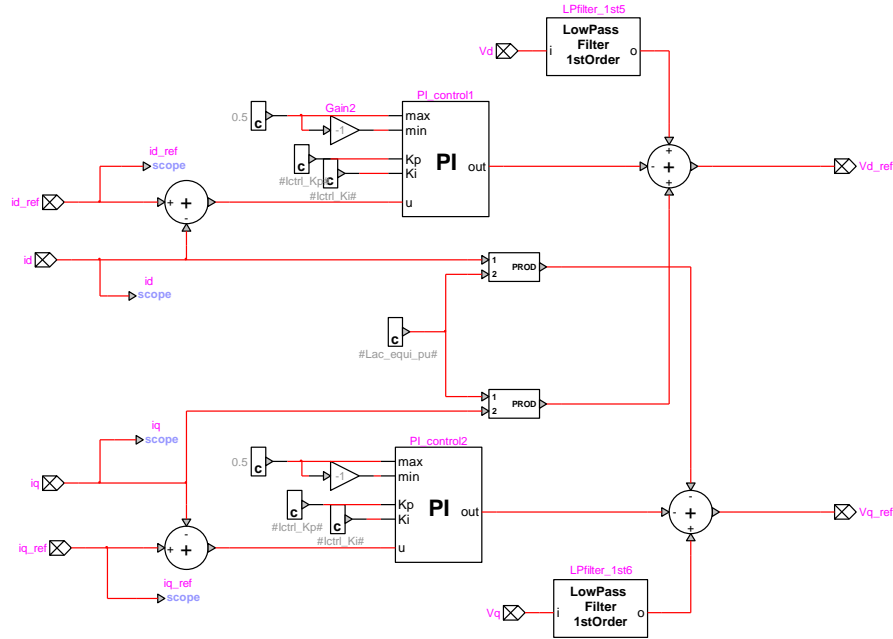


Figure 18: Inner Control

The outer controller is shown in Figure 19. It provides the reference currents (I_d_ref , I_q_ref) to the inner controller. From the main mask, the user can choose between three types of outer controls: active power control (P control), DC voltage control (V_{dc} control) and droop control (P/ V_{dc} control). The selector blocks

(violet color) are configured to automatically switch depending on the chosen control type. Also, in the main mask, the user can choose between reactive power control (Q control) and ac voltage control (Vac control). For the later, the selector is colored in pink to switch automatically form Q control and Vac control.

4.7.3.2.1 Active power control (P control)

As grid voltage vector is aligned with the d axis, the q component of the grid voltage is equal to zero and d component is equal to the voltage magnitude. Equation (15) becomes:

$$P = v_d i_d \quad (26)$$

An integral control is sufficient to produce the desired d current reference (I_{d_ref}). The control law of P control is defined respectively as:

$$i_{d_ref} = \frac{1}{v_d} \left(k_p + \frac{k_i}{s} \right) (P_{ref} - P) \quad (27)$$

4.7.3.2.2 DC voltage control (Vdc control)

From the MMC-AVM model (described in section 4.6.4) it can be found that SM capacitors can be represented as an equivalent capacitor C_{dc} . Since the energy in the equivalent inductance L_{DC} is small, it can be neglected. The following equation can be deduced

$$C_{dc} \frac{dV_{dc}}{dt} = i_d - I_{dc} \quad (28)$$

After neglecting the feed-forward component I_{dc} , a PI-control can be applied to regulate the DC voltage:

$$i_{d_ref} = \left(k_p + \frac{k_i}{s} \right) (V_{dc_ref} - V_{dc}) \quad (29)$$

4.7.3.2.3 P/Vdc Droop control

The Droop control functionality in the dc grid is similar to the Droop control in the ac grid. In the ac grid the relationship is between frequency and active power, in the dc grid the DC voltage is a function of active power and the droop coefficient is given by:

$$k_{droop} = \frac{\Delta V_{dc}}{\Delta P} \quad (30)$$

The active power delta is added over the active power reference (P_{ref}) as shown in Figure 19.

4.7.3.2.4 Reactive power control (Q control)

As the grid voltage vector is aligned with the d axis, the q component of the grid voltage is equal to zero and d component equal to the voltage magnitude. The equation (16) becomes:

$$Q = -v_d i_q \quad (31)$$

An integral control is sufficient to produce the desired q current reference (i_{q_ref}). The control law of Q control is defined as

$$i_{q_{ref}} = -\frac{1}{v_d} \left(\frac{k_i}{s} \right) (P_{ref} - P) \quad (32)$$

4.7.3.2.5 AC voltage control (Vac control)

From the reactive power equation(11), the voltage drop Δv_{grid} over the reactance (X_{PCC}) of the ac grid at PCC can be approximated as:

$$\Delta v_{grid} = v_s - v_{grid} \approx \frac{X_{PCC} Q}{v_s} \quad (33)$$

Since the grid voltage vector is aligned with the d axis and using (31), (33) becomes:

$$\Delta v_{grid} \approx X_{PCC} i_d \quad (34)$$

An integral control is sufficient to produce the desired q current reference (i_{q_ref}):

$$i_{q_{ref}} = -\left(\frac{k_i}{s} \right) (V_{ref} - V_{grid}) \quad (35)$$

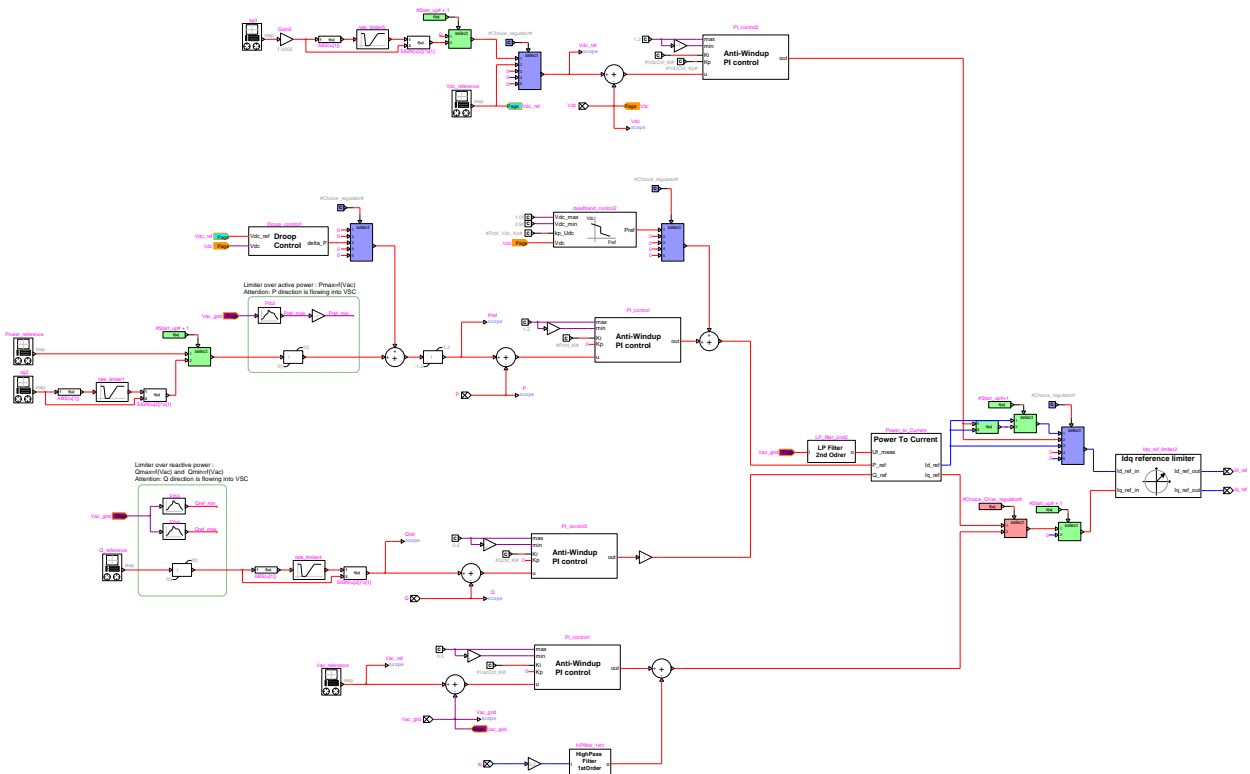


Figure 19: Outer Control block

When the start-up sequence is selected from the main mask, the reference values P_{ref} and V_{dc} have to be varied during simulation. Thus, the selectors colored in green are added in order to switch automatically from

constant references (used for normal operation of MMC station) to a time-domain varying reference (used for start-up sequence).

A current limiter is included in the outer control block in order to limit the converter current reference to a pre-set value. The current limiter control block is presented in Figure 20. The maximum converter currents are defined in the main mask. The user can choose between P or Q priority. The choice of which priority to choose will depend on the application. For instance, if the converter is connected to a strong grid used for transmission, the active reference current will be given high priority to produce more active power, when the current limit is exceeded. If the converter is connected to a weak grid or used to supply an industrial plant, the VSC will give high priority to the reactive reference current to keep up the ac voltage when the current limit is exceeded. The remaining capability is then available for active power production.

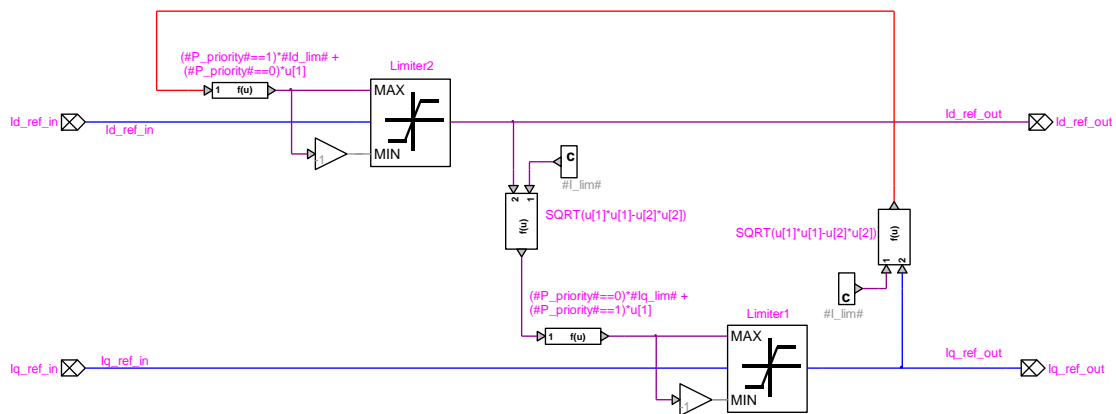


Figure 20: Current reference limiter – EMTP-RV

The synchronization block includes the internal oscillator and the PLL. Depending on the outer control type chosen from the main mask, the selector block (colored in violet) switches automatically between islanded and non-islanded operations.

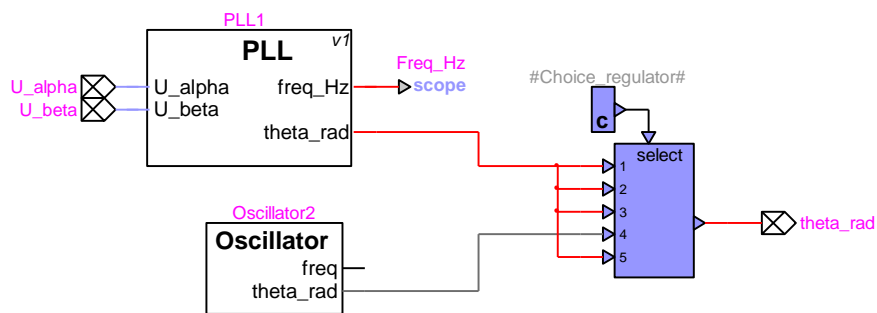


Figure 21: Synchronization - EMTP-RV

The main function of the PLL is to synchronize with the phase angle and frequency of the ac grid voltage. The grid voltage vector is chosen to align with the d axis reference. The PLL model is presented in Figure 22.

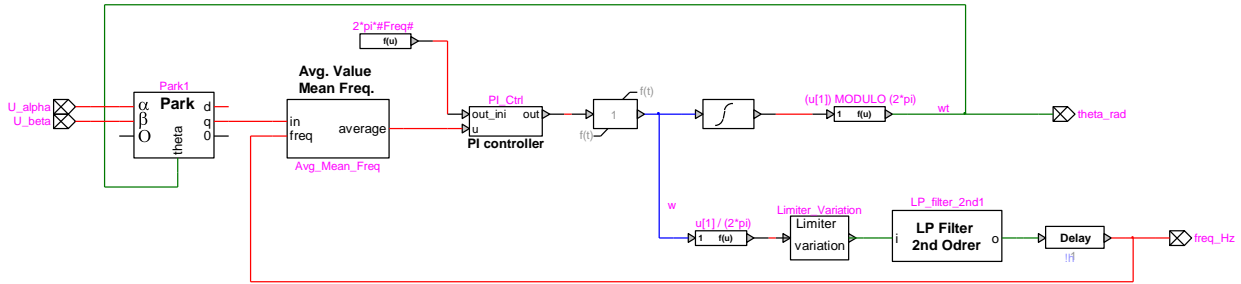


Figure 22: PLL Model

The internal oscillator is presented in Figure 23. It simply produces the phase angle.

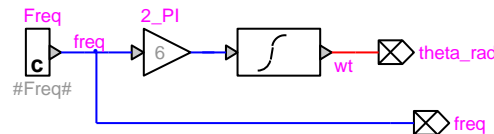


Figure 23: Internal oscillator

The magnitude of the reference vector V_{dq_ref} is linearized and limited at 1.5pu maximum value. The reference voltages are then converted to abc frame (V_{abc_ref}) as shown in Figure 24. Note that for P/Vdc droop control, the linearization is by-passed for better dynamic performance.

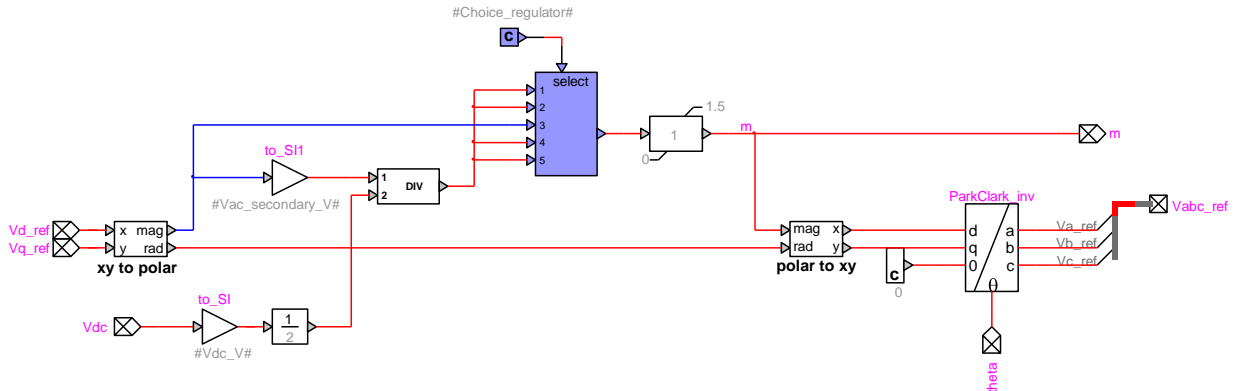


Figure 24: Linearization and dq to abc transformation

4.7.4 Lower Level Control

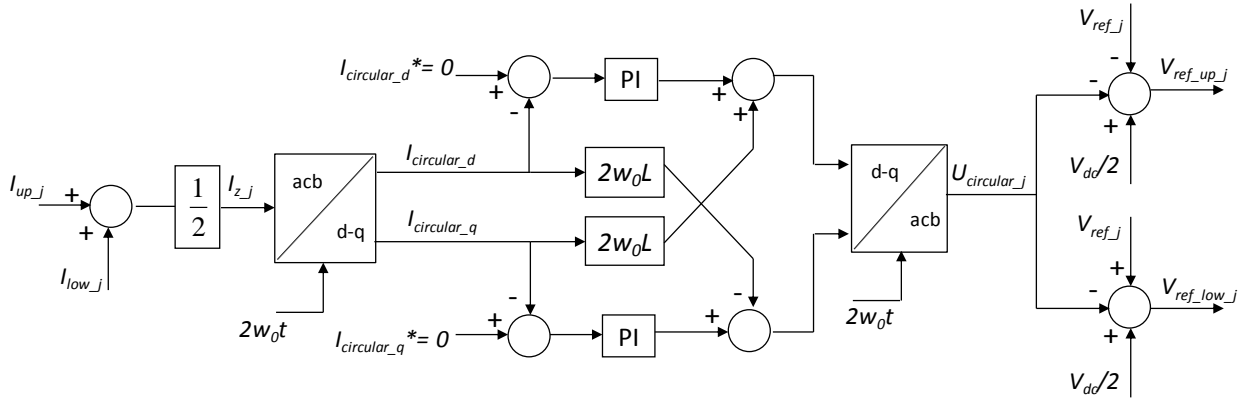
Unlike previous VSC technology, the MMC topology requires additional controllers in order to stabilize internal variables. The top level view of the control structure is presented in Figure 4.

The Lower Level Control block is hidden by means of a DLL block; hence, this control system is not accessible and cannot be modified by the user.

Lower level control is composed of: Circulating Current Suppression Control (CCSC), Nearest Level Control (NLC) modulation and Capacitor Balancing Algorithm (CBA). In this section, only a brief description is given for each main component.

4.7.4.1 Circulating Current Suppression Control (CCSC)

Voltage unbalances between the arm phases of the MMC introduce circulating currents containing a second harmonic component which not only distorts the arm currents, but also increases the ripple of SM capacitor voltages. Circulating currents can be eliminated by adding a parallel capacitor (resonant filter) between the mid-points of the upper and lower arm inductances on each phase [26] or using an active control over the ac voltage reference $v_{ref_{abc}}$ [25]. The latter is chosen in this control system.



7

Figure 25: Circulating Current Suppression Control (CCSC)

4.7.4.2 NLC modulation

Traditional modulation techniques proposed to date for MMCs include Phase-Disposition Modulation (PD-PWM), Phase-Shift Modulation (PS-PWM), Space-Vector Modulation (SV-PWM), and the improved Selective Harmonic Elimination method (SHE). As the number of levels increases in MMCs, PWM and SHE techniques become cumbersome for EMT-type simulations. Therefore, more efficient staircase-type methods, such as the Nearest Level Control (NLC) technique, can be used. The models developed in EMTP-RV use the NLC technique proposed in [25].

4.7.4.3 Capacitor Balancing Control

The capacitor voltage at all SMs must be balanced and kept the same during normal operation. To achieve this, the capacitor voltage (Figure 3.a) must be monitored and switched ON and OFF based on a Balancing Control Algorithm (BCA). The BCA measures the capacitor voltages at each SM at any instant and sorts them before selecting the upper and lower SM to switch ON. The number of SMs is determined based on the $N_{up}(t)$ and $N_{low}(t)$ switching functions, where $N_{up}(t) + N_{low}(t)$ corresponds to the total number of SMs per arm. To improve the efficiency of the algorithm, the model includes a trigger control that activates the BCA only when a new (ON/OFF) state in the $N_{up,low}(t)$ functions is reached. This will avoid switching the SMs at each time step.

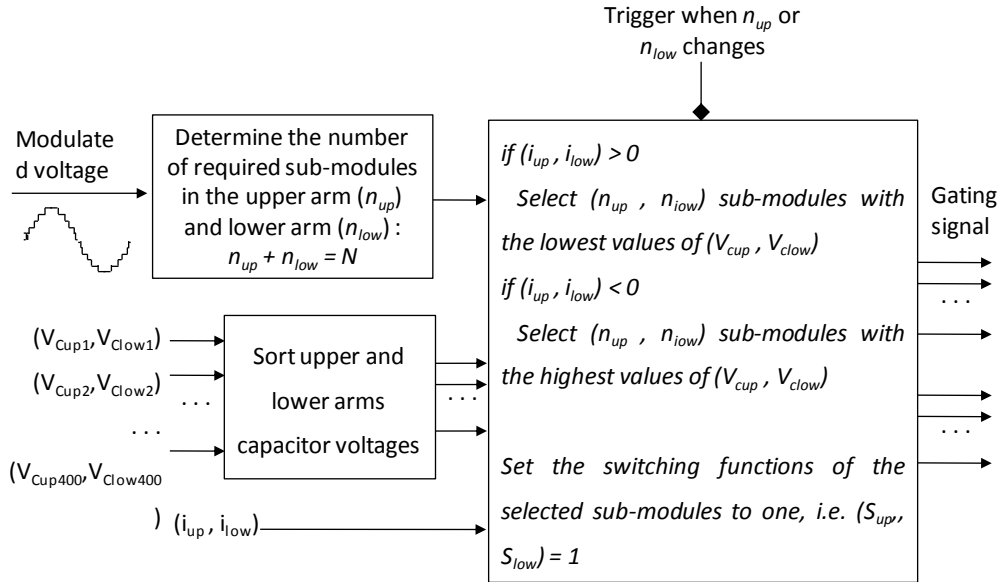


Figure 26: Balancing control algorithm (BCA)

It is noted that, all these controllers are included when the MMC Model 1 (Full detailed) and Model 2 (Detailed equivalent) are chosen from the main mask. However, if the Model 3 (Switching function of Arm) is selected, the BCA device is excluded from the Lower Level Control and if the Model 4 (AVM) is selected, the Lower Level Control is not represented.

4.8 Protection System

The protection system includes dc overcurrent and Deep voltage sag detectors (see Figure 27). The protection system can be activated or deactivated from the main mask. During initialization, i.e. all protection systems are activated after 300 ms of simulation (i.e. $init_Protection = 0.3s$).

When the dc current is higher than the maximum current limit set in the main mask, the MMC station is tripped: the MMC is blocked and main ac breaker is opened. When grid voltage is lower than 0.1 pu, the MMC is blocked with a release delay of 20 ms.

When the start-up sequence is activated from the main mask, the closing times of both breakers (ac breaker and converter breaker, see Figure 1) are set in this device.

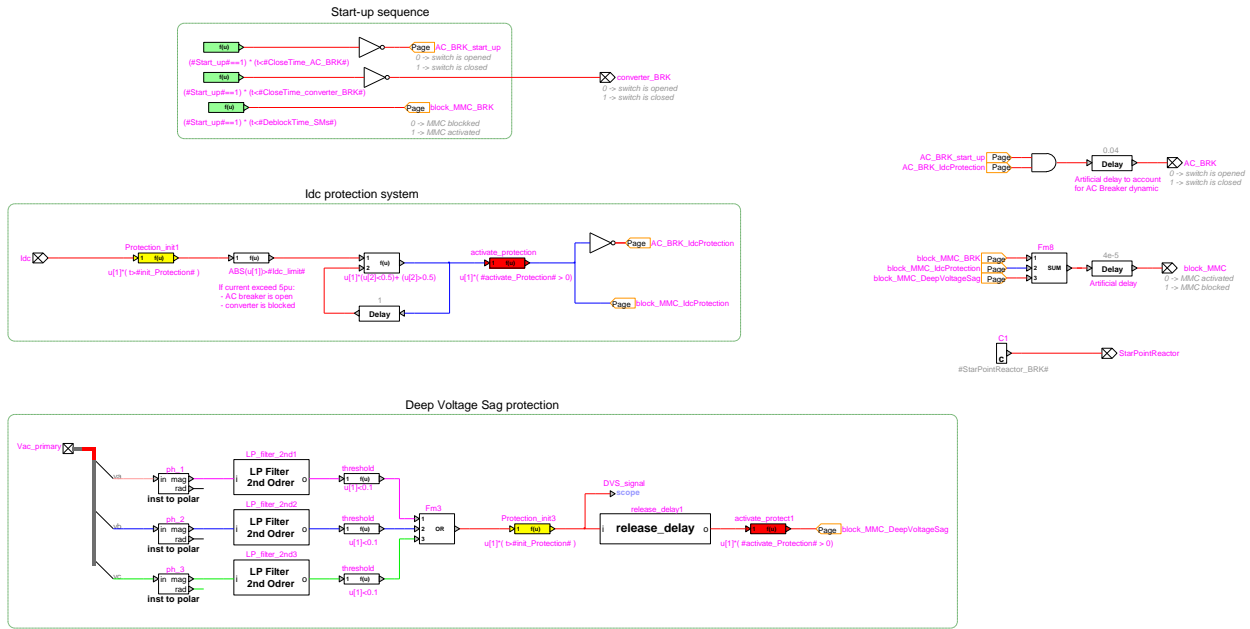


Figure 27: Protection system and Start-up sequence

4.9 Start-up sequence

When the Start-up Sequence is unchecked, at simulation $t=0$:

- the initial Capacitor voltage of each SM (v_{C_i}) is set to nominal voltage
- the main ac breaker is closed
- the ac converter breaker is closed
- the SMs are at deblock state
- the P and Vdc references are set at their desired values (Pref, Vdc_ref)

When the Start-up sequence is checked, 6 parameters have to be configured:

- closing time of ac breaker
- closing time of ac converter breaker
- deblocking time of SMs
- ramping start time dc voltage reference
- time to switch from Vdc-Control to P-control
- start time ramping of active power reference

4.10 Initial Conditions and Load-flow solution

For the load-flow solution the MMC station model is represented by a PQ constraint (Figure 28). The PQ constraint is set from the main mask. The voltage source (PQ_init) initializes the steady-state operation with the load-flow parameters and is disconnected from the system after the “initialization time” set in the main mask.

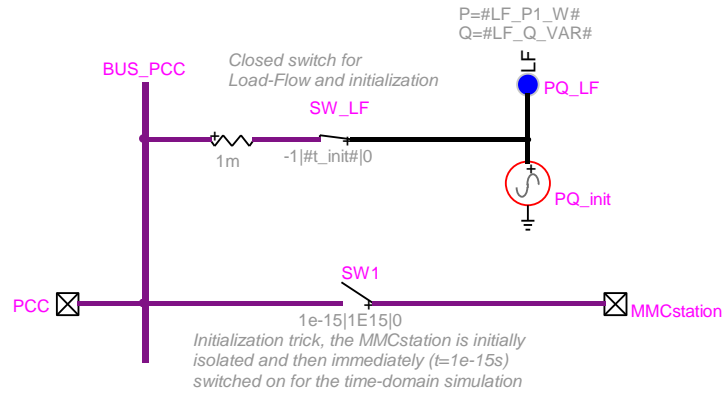


Figure 28: Load-flow and initialization - EMTP-RV

5 Simulation results

This section provides a comparison between the four types of MMC models: Model 1, 2, 3 and 4. The dynamic behavior comparison is conducted for step-change of active power reference, three-phase: ac fault, pole-to-pole DC fault and start-up sequence [10].

The studied system is presented in Figure 29 and is available in the Examples folder of EMTP-RV. The control strategy considers an active/reactive power control on the sending end (VSC_1) and a dc voltage/reactive power control on the receiving end (VSC_2). The ac grids are represented as equivalent sources with a short-circuit level of 10,000 MVA. The transmission capacity of the system is 1,000 MW from S1 to S2. The DC cable is modeled using a wideband line model [27]. Each MMC station considers a 401-level MMC (400 SMs/arm). The Model 1 (with nonlinear IGBT/diode model) constitutes the reference model.

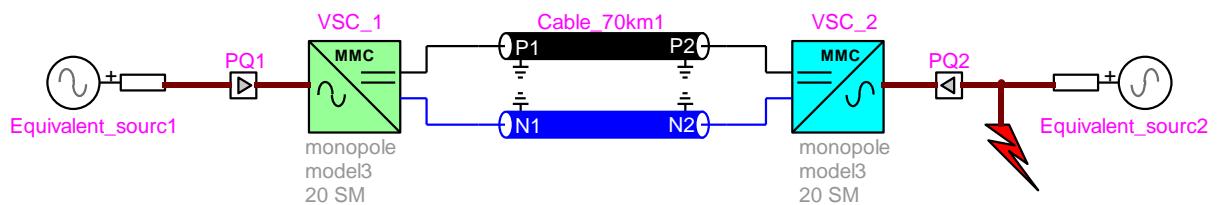


Figure 29: MMC-HVDC transmission test system

5.1 Step change on active power reference

A step change in the active power reference for VSC_1 is applied at 0.5 s of simulation. The active power reference is reduced from 1 to 0.5 pu. In Figure 30 all four models deliver identical results. Figure 31 presents internal variables related to the studied MMC topology. The difference current in phase A is defined as

$$i_{diff_a} = (i_{u_a} + i_{l_a}) / 2 \text{ and the sum of all capacitor voltages of each arm of phase A are given by } v_{C_{totua}} \text{ and } v_{C_{totla}},$$

respectively (see Figure 3). Since arm details are not represented in Model 4 (see Figure 13), only Models 1, 2 and 3 are compared here. As it can be noticed, the three models give similar and accurate results.

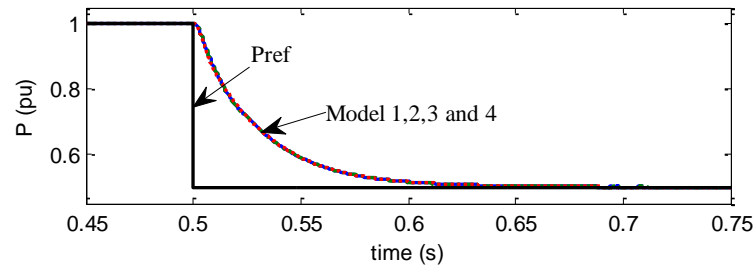
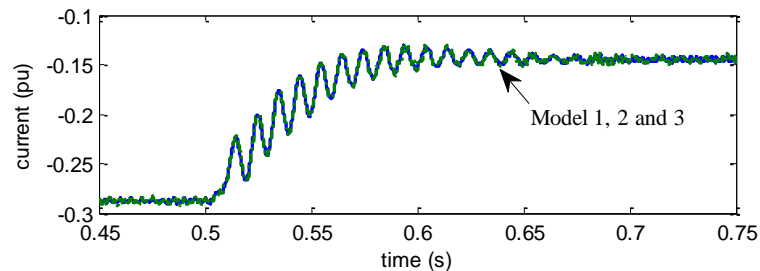
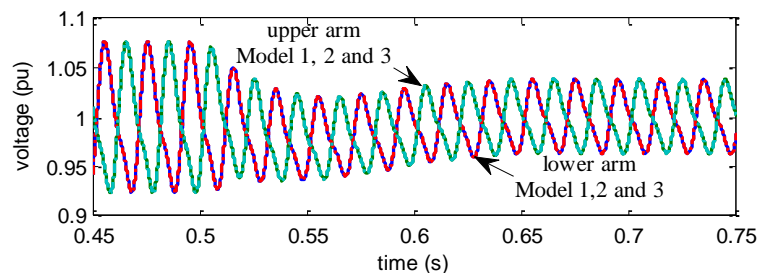


Figure 30: Active power responses, power flowing into VSC_1



a) VSC_1 phase A, difference current i_{diff_a}

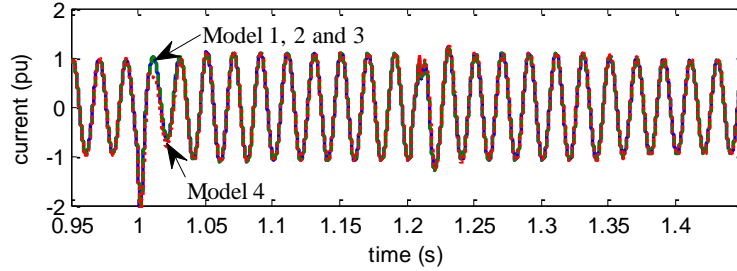


b) VSC_1 phase A upper and lower arms, $v_{C_{tot}}$

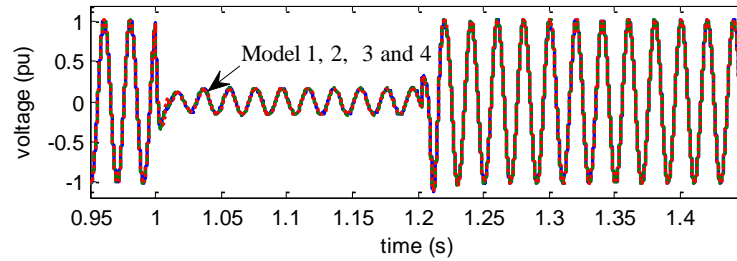
Figure 31: Step change in active power reference for VSC_1

5.2 Three-phase ac fault

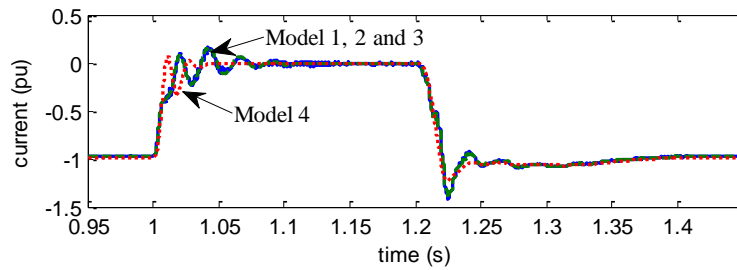
A 200 ms three-phase-to-ground fault is applied on the ac side of VSC_2 (see Figure 29) at 1 s of simulation time. Figure 32 compares the dynamic responses. The results from Models 2 and 3 are similar to Model 1, and Model 4 remains sufficiently accurate. Figure 32.d shows an attenuated oscillation around 413 Hz during the fault, which has slightly higher amplitude (peak-to-peak mean value 0.008 pu) in Models 1 and 2 than in Model 3 (peak-to-peak mean value 0.001 pu). This oscillation is related to the interaction between the MMC and the dc cable. The current increases rapidly during the ac fault. The capacitor voltage fluctuations of each SM will also increase and the assumption in equation (2) will become less accurate. This transient generates harmonics in the MMC that interact with the dc cable.



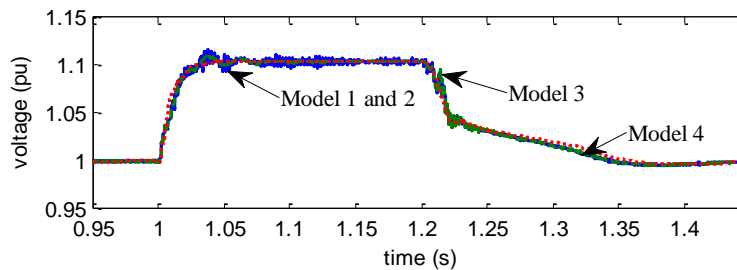
a) VSC_2 phase A current i_a



b) VSC_2 phase A voltage v_a



c) VSC_2 dc current I_{dc}



d) VSC_2 dc voltage V_{dc}

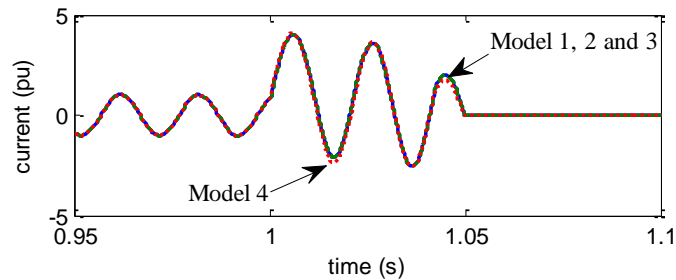
Figure 32: Three-phase ac fault, 401 levels, blue line for Models 1 and 2, green line for Model 3 and red line for Model 4.

5.3 Pole-to-pole dc fault

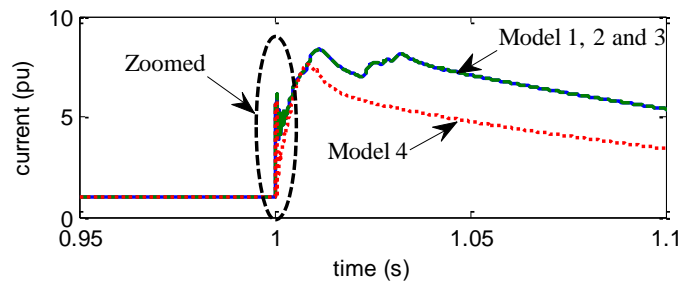
The models are tested for a permanent dc fault between the positive and negative poles in the middle of the dc cable. The fault is applied at 1.9 s. Since the protection system is activated, the ac breaker is opened and the MMCs are blocked after fault occurrence. The dc and ac currents in VSC_1 are compared in Figure 33 for

different models. The dc current peak during a pole-to-pole fault reaches a value of approximately 8.2 pu for Models 1 to 3. A peak value of 7.3 pu is reached with Model 4. However, the ac waveforms of Model 4 are close to the other models.

From the zoomed waveform of Figure 34, it can be noticed, that just after the dc fault occurrence, Model 4 accurately mimics the slope and peak values of I_{dc} . However, after around 1 ms, the behavior becomes different, due to the inaccurate representation of the MMC blocked state in Model 4.



a) VSC_1 ac current: i_a



b) VSC_1 dc current: I_{dc}

Figure 33: DC fault results blue line for Models 1 and 2, green line for Model 3 and red line for Model 4

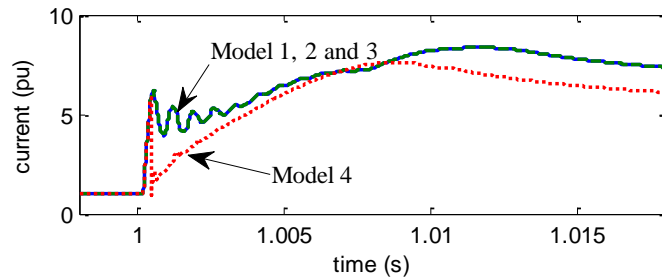
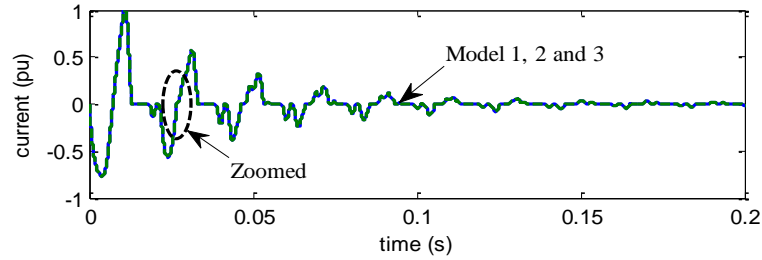


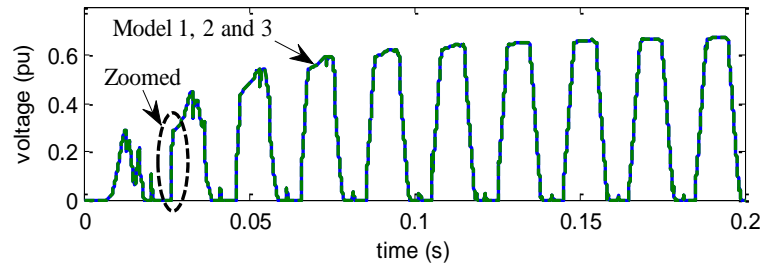
Figure 34: Zoomed waveform, VSC_1, I_{dc}

5.4 Start-up sequence

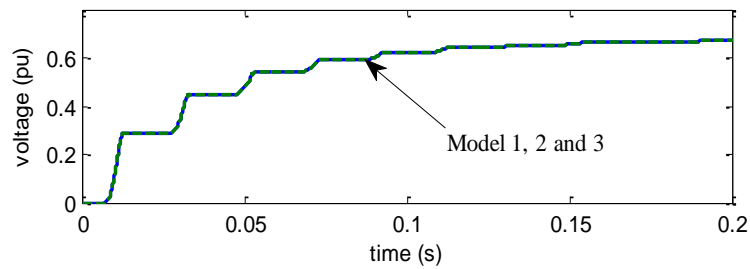
The start-up sequence procedures of all MMC stations are activated for this simulation. In this report, only the first 200 ms of simulation are shown. However, the entire start-up sequence example is available in the example folder: "MMC_HVDC_link_StartUp.ecf". Since arm details are not represented in Model 4 (Figure 13), this model cannot be used to study start-up. Only Models 1, 2 and 3 are compared in this document.



a) VSC_1 phase A; upper arm current i_{u_a}



b) VSC_1 phase A; upper arm voltage v_{u_a}

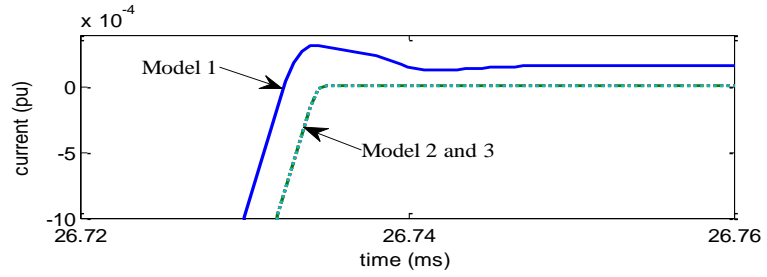


c) VSC_1 phase A; upper arm $v_{C_{tot_{u_a}}}$

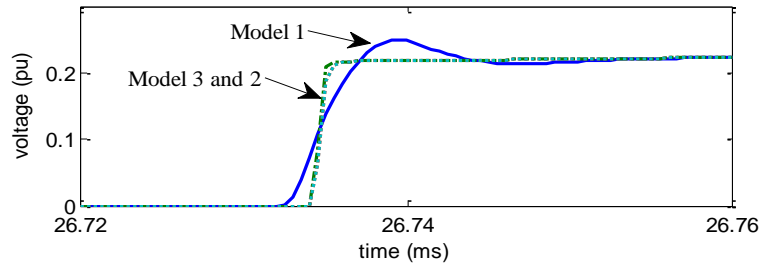
Figure 35: VSC_1 phase A variables, start-up sequence, 401 levels

Since in Figure 35 both Models 2 and 3 are able to match the results from Model 1, it is concluded that these two simplified models can be used to study converter start-up.

The zoomed waveforms of Figure 36 are used to highlight the detailed modeling effect of power switches in Model 1. It is observed that Model 1 mimics the reverse recovery behavior of diodes, whereas in Models 2 and 3 this behavior cannot be represented due to the linear representation of power switches.



b) Zoomed waveform VSC_1 phase A, upper arm current i_{u_a}



b) Zoomed waveform VSC_1 phase A, upper arm voltage v_{u_a}

Figure 36: Zoomed waveform VSC_1, phase A variables for start-up sequence

6 References

- [1] N. Flourentzou, V. G. Agelidis and G. D. Demetriades, "VSC-Based HVDC Power Transmission Systems: An Overview," *IEEE Trans. on Power Electronics*, vol. 24, no. 3, pp. 592-602, March 2009.
- [2] "It is time to connect, Technical description of HVDC Light technology," ABB, Sweden, March 2008.
- [3] U. Karaagac, J. Mahseredjian, H. Saad, S. Jensen and L. Cai, "Examination of Fault-Ride-Through Methods for Off-Shore Wind Farms Connected to the Grid through VSC-Based Multi-terminal HVDC Transmission", *IPST 2013, International Conf. on Power Systems Transients*, Vancouver, Canada, 18-20 July 2013.
- [4] A. Lindberg, "PWM and Control of Two and Three level High Power Voltage Source Converters," *Licentiate Thesis, Royal Institute of Technology*, Stockholm, Sweden, 1995.
- [5] C. Du, "VSC-HVDC for industrial power systems," Ph.D. Thesis, Chalmers Univ. of Technology, Göteborg, Sweden, 2007.
- [6] B. R. Andersen, L. Xu, and K. T. G. Wong, "Topologies for VSC transmission," 7th International conference on AC-DC Power Transmission, pp. 298-304, London, Nov. 2001.
- [7] A. Lesnicar and R. Marquardt, "An Innovative Modular Multilevel Converter Topology Suitable for a Wide Power Range," *Proc. IEEE Power Tech. Conference*, vol. 3, Bologna, June 2003.
- [8] B. Gemmell, J. Dorn, D. Retzmann, and D. Soerangr, "Prospects of Multilevel VSC Technologies for Power Transmission," *Proc. IEEE Transmission and Distribution Conf. Exp.*, Milpitas, CA, Apr. 2008, pp. 1-16.
- [9] J. Peralta, H. Saad, S. Denetiere, J. Mahseredjian and S. Nguéfeu, "Detailed and Averaged Models for a 401-level MMC-HVDC system" *IEEE Trans. on Power Delivery*, vol. 27, no. 3, July 2012, pp. 1501-1508.
- [10] H. Saad, S. Denetiere, J. Mahseredjian, P. Delarue, X. Guillaud, J. Peralta, S. Nguéfeu, "Modular Multilevel Converter Models for Electromagnetic Transients," *accepted for IEEE Trans. on Power Delivery*, TPWRD-00396-2013.R1.
- [11] U. Karaagac, H. Saad, J. Mahseredjian, S. Jensen, L. Cai, "Off-Shore Wind Power Plant Modeling Precision and Efficiency in Electromagnetic Transient Simulation Programs," 11th International Workshop on Large-Scale Integration of Wind Power into Power Systems, Lisbon, Portugal, Nov. 13-15, 2012.
- [12] J. Peralta, H. Saad, S. Denetiere, J. Mahseredjian, "Dynamic performance of average-value models for multi-terminal VSC-HVDC systems," *Proc. of IEEE Power Engineering Society General Meeting*, San Diego, 2012, 10.1109/PESGM.2012.6345610.
- [13] L. G. Franquelo, et al., "The Age of Multilevel Converters Arrives," *IEEE Industrial Electronics Magazine*, vol. 2, no. 2, pp. 28-39, June 2008.

- [14] A. Antonopoulos, L. Angquist, and H. P. Nee, "On Dynamics and Voltage Control of the Modular Multilevel Converter," 13th European Conf. on Power Electronics and Applications, Barcelona, Oct. 2009.
- [15] B. T. Ooi and X. Wang, "Voltage angle lock loop control of the boosted type PWM converter for HVDC application," *IEEE Trans. Power Electron.*, vol. 5, no. 2, pp. 229–235, Apr. 1990.
- [16] J. Svensson, "Voltage angle control of a voltage source inverter, application to a grid-connected wind turbine," Proc. 6th Eur. Conf. Power Electronics and Applications, Sevilla, Spain, 1995.
- [17] M. P. Kazmierkowski and L. Malesani, "Current control techniques for three-phase voltage-source PWM converters: A survey," *IEEE Trans. Industrial Electron.*, vol. 45, no. 5, pp. 691–703, Oct. 1998.
- [18] H. Saad, J. Peralta, S. Denneriere; J. Mahseredjian, et al., "Dynamic Averaged and Simplified Models for MMC-Based HVDC Transmission Systems," *IEEE Transactions on Power Delivery*, vol. 28, no. 3, pp. 1723-1730, July 2013.
- [19] H. Jin, "Behavior-mode simulation of power electronic circuits," *IEEE Trans. On Power Electronics*, vol. 12, no. 3, pp. 443-452, May 1997.
- [20] S. R. Sanders, J. M. Noworolski, X. Z. Liu and G. C. Verghese, "Generalized Averaging Method for Power Conversion Circuits," *IEEE Trans. on Power Electronics*, vol. 6, no. 2, pp. 251-259, Apr. 1991.
- [21] H. Saad, C. Dufour, J. Mahseredjian, S. Dennerière and S. Nguéfeu, "Real Time simulation of MMCs using the State-Space Nodal Approach", IPST 2013, International Conf. on Power Systems Transients, Vancouver, Canada, July 18-20, 2013.
- [22] H. Ouquelle, L. A. Dessaint, S. Casoria, "An Average Value Model-Based Design of a Deadbeat Controller for VSC-HVDC Transmission Link," *IEEE Power Energy Soc. Gen. Meeting*, pp. 1-6, Calgary, July 2009.
- [23] C. Edwards, I Postlethwaite, "Anti-windup and bumpless-transfer schemes," *Automatica*, vol. 34, Issue 2, February 1998, pp. 199-210
- [24] L. Zhang, "Modeling and Control of VSC-HVDC Links Connected to Weak AC Systems," Ph.D. Thesis, *Royal Institute of Technology*, Stockholm, Sweden, 2010.
- [25] Q. Tu, Z. Xu, and L. Xu, "Reduced Switching-Frequency Modulation and Circulating Current Suppression for Modular Multilevel Converters," *IEEE Trans. on Power Delivery*, vol. 23, no. 3, pp. 2009-2017, Jul. 2011.
- [26] B. Jacobson, P. Karlsson, G. Asplund, L. Harnefors, T. Jonsson, "VSC-HVDC Transmission with Cascaded Two-Level Converters," *CIGRE Conference*, Paris, pp. B4–110, Aug. 2010.
- [27] A. Morched, B. Gustavsen, M. Tartibi, "A Universal Model for Accurate Calculation of Electromagnetic Transients on Overhead Lines and Underground Cables", *IEEE Trans. on Power Delivery*, vol. 14, no. 3, pp. 1032–1038, July 1999.